UNIVERSITY OF BIRMINGHAM

Modelling wind fields and debris flight in tornadoes

Baker, C. J.; Sterling, M.

Link to publication on Research at Birmingham portal

Modelling wind fields and debris flight in tornadoes

C.J. Baker [*], M. Sterling

School of Engineering, University of Birmingham, Edgbaston, Birmingham, B15 2TT, United Kingdom

A B S T R A C T

This paper describes the derivation of a simple yet realistic engineering model of tornado wind and pressure fields. This novel model is shown to be capable of providing a method for predicting wind speed and pressure time histories and debris impact energies that can ultimately be used in the development of a rational risk-based design methodology for tornado wind loads on buildings. A stationary one-cell tornado vortex is first considered, and the circumferential and vertical velocities and pressure profiles derived from a simple assumption for radial velocity (that is bounded in the radial and vertical directions) and the use of the Euler equations. The generalisation of this model to a two-cell tornado form is then set out. This model is then used to investigate the trajectories of wind borne debris in tornado wind fields, and for the first time, this analysis reveals the important dimensionless parameters of the problem and the parameter boundary between falling and flying debris. An asymptotic long time solution for debris paths is also derived.

1. Introduction

Tornadoes are complex meteorological phenomena often associated with severe convective atmospheric conditions. In simple terms they consist of a swirling circumferential flow, a radial inflow or outflow, and a vertical flow component. Wind speeds for the most severe tornadoes can reach 100 m/s. It is a well-observed fact that, in some parts of the world, severe tornadoes can cause significant structural damage and loss of life. That being said, most of the efforts of the engineering community over the last few decades have concentrated on predicting and designing for the wind loads from large scale synoptic storms, and until recently little attention has been given to the wind loads due to tornadoes and other small scale convective storm types, and only the crudest of design procedures have been established for such storms, usually based on simple maximum wind speeds. Until recently there was a tendency to assume that the effects of wind (regardless of its origin) would be largely the same – an assumption which has been demonstrated to be incorrect (Jesson et al., 2015). In recent years however the situation has changed, and there is ongoing work to determine the structure of tornadoes from field tests (eg Bluestein et al., 2003); in the development of model scale tornado vortex generators which can be used to give surface pressure data on structures during tornado events (eg. Haan et al., 2008, Mishra et al., 2008a,b, Case et al., 2013, Hangan and Kim (2008), Hashemi-Tari et al. (2010), Refan and Hangan (2016)); and also some investigators

have used unsteady CFD methods to predict tornado wind fields (eg Ishihara et al., 2011). These investigations have significantly enhanced the understanding of tornado wind load effects through giving insight into the nature of tornado wind flows. Also in recent years much work has been carried out on the calibration of physical models against full scale data by both laboratory specialists and full scale experts (e.g. Refan et al., 2014).

Essentially there are three types of loading caused by the passage of a tornado over a structure – loads directly related to the flow over the structure resulting in time varying surface pressure fields; loads due to the difference in the rapidly changing low pressure in the tornado core, and the higher, less rapidly changing pressures within buildings; and impact loads due to impact of the flying debris that is often found in tornadoes. Tornado loading is usually taken into account only for highly sensitive structures such as nuclear power plants. The methodology used in the US nuclear industry is given in USNRC (2007). This is based on maximum wind speeds of a specified risk, pressure drops calculated from a simple Rankine vortex model (see below) and debris impact velocities for a restricted range of debris types from numerical trajectory models. However, a conceptual method of how all these essentially time varying effects could be incorporated into design for a range of risk levels is yet to be developed, although there is some ongoing work by Tamura et al. (2015) that is attempting to build a tornado database for use in design in Japan. It is nonetheless clear that a pre-requisite of such a method would

---

be a consistent and simple description of the tornado flow field that could be used in design to predict velocity and pressure time histories and to enable debris trajectories to be calculated. In this paper we set out the development of such a simple analytical model of tornado wind and pressure fields that has the potential to meet these needs and apply these models to the calculation of debris trajectories.

Section 2 of this paper describes the available full-scale data for tornado wind and pressure fields and recent work in debris trajectory modelling. Section 3 firstly develops an analytical model for a stationary one-cell tornado, based on a solution of the high Reynolds number Navier-Stokes equations (Euler equations) for wind and pressure distributions, and validates it against full scale data as far as possible. A more complex two-cell formulation with a central downdraft is also set out. Section 4 then considers debris flights in tornadoes, identifying the major dimensionless parameters that are of importance, and calculating debris trajectories over a wide parameter range. The parameter boundary between flying and falling debris is defined. An asymptotic analysis of debris trajectories is also presented. Finally some concluding remarks are set out in section 5.

2. Earlier investigations

2.1. Full scale data

In the modelling work we describe below, we base the development of the model on available, if rather sparse, full scale data. We have not attempted to relate the model to computational of physical model simulations of tornadoes as these are themselves models of a complex reality. Such data has been measured for a number of decades, mainly using radar techniques (eg Wurman et al., 1996; Wurman and Gill, 2000; Bluestein et al., 2003; Lee and Wurman, 2005; Sarkar et al., 2005). These are able to give some details of the tornado structure in terms of geometric scale and wind speeds and directions, but are unable to give a great deal of detail of tornado structure near the ground, which is of course of most interest to wind engineers. Sometimes, usually fortuitously, surface pressure measurements were taken (Lee and Samaras, 2004; Karstens et al., 2010). From this data the following broad conclusions could be drawn.

- Whilst the classic single cell tornado (radial inflow and central updraft) was often observed with circumferential circulation, multi-cell tornadoes also exist, some with downdrafts in the central core that may or may not extend to ground level. Multi-cell tornadoes have been observed more often than single cell ones.
- Tornadoes are very transitory, with properties varying through the life of the tornado.
- Maximum tangential wind speeds of 90–110 m/s have been recorded, but for most tornadoes the wind speeds are significantly lower.
- The core radius (the distance from the centre to the maximum tangential velocity) is of the order of 50–200 m.
- The translational velocities are of the order of 5–15 m/s.

More recently Refan et al. (2014) have collated a large dataset of tornado wind speeds measured by the Ground Based Velocity Track Display technique (Lee at al 1999). These were for relatively low wind speed tornadoes, with maximum wind speeds between 36 and 62 m/s, but nonetheless do give detailed circumferential velocity distributions over a range of heights. The data, which is for both single-cell and two-cell tornadoes, will be used to verify the new model later in the paper.

At this point it is worth pointing out that there are two aspects of tornado flows about which there is very little information, and which will be seen to be important in what follows. The first is that of the near ground boundary layer, where the velocity will increase from zero to some "free stream" value. This must exist physically, but to the author's knowledge no information on its form is available. The second is the turbulent statistics of the tornado. One would expect small scale turbulent eddies to exists within the overall flow structure, but again there seems to be little information available on this from full-measurements, although there are a number of (unverified) model-scale datasets.

2.2. Debris flight

The damage caused by flying debris in tornadoes is clear from a study of the damage investigations that have taken place in recent years – see for example Brooks and Doswell (2001), and this subject has been studied since the 1970s. Lee (1974), Redmann et al. (1976) and Twisdale et al. (1979) all developed wind field models and trajectory models that described debris flight in tornadoes. The wind field models however were essentially empirical relationships that sought to capture some of the main features of tornadoes, and were not set in a consistent analytical framework. Similarly the debris flight models were also somewhat ad hoc and lacked a general framework and thus their use in design was limited. Nonetheless these models were used to predict impact velocities from missiles in tornadoes that proved to be the basis for codification and testing over the following decades (McDonald, 1990). In the early years of this century, a number of authors considered the issue of debris flight afresh, and consistent analytical frameworks were developed – see for example the work of one of the authors in Baker (2007), although this is only one of a number of similar investigations. Of perhaps most significance was the formal definition of three types of debris – compact with all three dimensions similar in magnitude, sheet – flat plates defined by two dimensions; and rod – with one dimension much greater than the others. Also the importance of the dimensionless parameter known as the Tachikawa number (Holmes et al., 2006), which is based on the early work of Tachikawa (1988) in Japan, has been recognised. This is essentially the ratio of the inertial forces in the flow to the weight of the debris. More recently the focus of engineering tornado studies has turned to physical and numerical simulation (Mishra et al., 2008a, b; Sarkar et al., 2005). With regard to the latter, two recent investigations have also looked at the flight of debris in tornadoes – Maruyama (2011) and Noda et al. (2015) using Large Eddy Simulation, and whilst these results are interesting and give a very great deal of the flow fields and trajectories, the resources required mean that the simulations are somewhat idealised and uncalibrated (often attempting to match the geometry of physical models) and present the results for only a small number of cases.

3. The tornado model

3.1. Existing tornado wind models

In this section we briefly consider the analytical formulations of tornadoes that have been previously proposed by earlier workers. The simplest of these is the Rankine vortex, which effectively consists of a forced vortex core and a free vortex outer region. The circumferential velocity field is given by

$$r < r_m \quad V = \frac{V_m r}{r_m} \quad r > r_m \quad V = \frac{V_m r_m}{r} \tag{1}$$

where $V = V_m$ is the maximum velocity at a radius $r = r_m$. Note that no radial or vertical velocities are specified and thus for the purposes set out in section 1 (the calculation of loads and debris trajectories), it is not of any use, although a number of authors have shown it is a good fit to some full scale data (Wood and Brown, 2011). Also note that there is a sharp discontinuity at $r = r_m$. This model is however used in the loading methodology of USNRC (2007). A rather more complex formulation of tornado flows is offered by the Burgers-Rott vortex model (Burgers, 1948; Rott, 1958), which is a solution of the full Navier-Stokes equations. This begins from the assumption that the radial velocity is an inflow with a magnitude proportional to the radial distance. Applying the continuity and circumferential momentum equations then leads to the following

expressions for the radial, circumferential and vertical velocities U, V and W respectively.

$$U = -ar \quad V = \frac{\Gamma}{2\pi r}\left(1 - e^{-\left(\frac{ar^2}{\nu}\right)}\right) \quad W = 2az \tag{2}$$

where a is a constant of proportionality, Γ is a circulation and ν is the kinematic viscosity. Again the circumferential velocity form has been found to be a good fit to some observed data by a number of authors (Wood and Brown, 2011). At low and high values of the radius it tends to the form of the Rankine vortex model outlined above. Note that this exact solution of the Navier-Stokes equations is essentially a viscous solution, and is thus only strictly valid for laminar, low Reynolds number flow. The author applied it in this way to the core of a laminar horseshoe vortex around the bases of wall mounted in cylinders in 1978 for vortex Reynolds numbers of 10–100 (Baker, 1978), where the scale of the vortex was only of the order of a centimetre. To apply it to the tornado situation in effect requires the assumption of a constant eddy viscosity throughout the flow field at much higher Reynolds numbers. This effect can be masked by normalising the velocities with the maximum V velocity, but the viscous nature of the solution still remains. This point being made however, the model is still not useful for our current purposes, because the radial and vertical velocity fields have no outer bounds and can only be realistic close to the centre of the tornado. A significantly more complex model is the solution of the Navier-Stokes equation developed by Sullivan (1959). This has a two-cell solution, expressed in terms of rather complex integrals, with a downdraft in the centre and an updraft in an annular ring, and is again a viscous solution whose application to the tornado situation requires the assumption of constant eddy viscosity. Again there is no bound on the U and W velocities in the radial direction, which makes it unsuitable for practical purposes. Finally mention must be made of a range of other models such as those of Fujita (1978) and Xu and Hangan (2009), which are empirical patched model of different analytical formulations for different aspects of the flow. As these are not in general consistent with the Navier Stokes equations, they will not be considered further here.

3.2. The nature of the model

Based on the summary of full-scale measurements set out in section 2, a new wind field model for a one-cell tornado has been developed which has the following characteristics.

- A single cell vortex with radial inflow and vertical upflow.
- The radial inflow with a maximum in the radial direction at $r = r_m$ and falls to zero at $r = 0$ and $r = \infty$.
- The radial inflow has a maximum in the vertical direction at $z = z_m$, and falls to zero at $z = 0$ and $z = \infty$.
- The velocity and pressure fields are solutions of the Euler equations - the inviscid, high Reynolds number, Navier-Stokes equations.

Section 2 identified two unknowns – the nature of the tornado boundary layer, and the nature of tornado turbulence. With regard to the former, we model this through allowing the radial velocity to increase from zero at the ground to a maximum value at $z = z_m$. With regard to the latter, we simply assume that the turbulence can be neglected, which seems preferable to the assumption of a constant eddy viscosity used in the other formulations described in the last section.

3.3. Velocity fields

We adopt the following form for the radial velocity field (the form being chosen because it permits a solution of the Euler equations – see below).

$$\overline{U} = \frac{-4\overline{r}\overline{z}}{(1 + \overline{r}^2)(1 + \overline{z}^2)} \tag{3}$$

Here, $\overline{U} = U/U_m$, where U is the radial velocity; $\overline{r} = r/r_m$ and $\overline{z} = z/z_m$ and r and z are the radial and vertical distances from the centre of the vortex. We thus assume that the velocity is normalised with a reference radial velocity U_m, and that the lengths are normalised with the radial and vertical lengths (i.e., r_m and z_m respectively at which this reference velocity occurs). This represents an inflow into the tornado centre, with a maximum value of the inflow at $\overline{r} = \overline{z} = 1$, with the reference velocity in this case representing the maximum radial velocity. It shows a peak in radial velocity both in the radial and vertical directions, and the velocity goes to zero at the core and at infinity in a physically plausible way.

The continuity equation and the circumferential momentum Euler equations are then written in dimensionless form as follows, with the viscous terms being ignored in the latter.

$$\frac{1}{\overline{r}}\frac{\partial(\tilde{U}\overline{r})}{\partial\overline{r}} + \frac{1}{\delta}\frac{\partial\overline{W}}{\partial\overline{z}} = 0 \tag{4}$$

$$\overline{U}\frac{\partial\overline{V}}{\partial\overline{r}} + \frac{\overline{U}\overline{V}}{\overline{r}} + \frac{\overline{W}}{\delta}\frac{\partial\overline{V}}{\partial\overline{z}} = 0 \tag{5}$$

where $\overline{V} = V/U_m$, $\overline{W} = W/U_m$, where V and W are the circumferential and vertical velocities respectively and $\delta = z_m/r_m$. δ is thus the ratio between the vertical and horizontal length scales. Using the radial velocity assumption and making the assumption that $\overline{V} = f(\overline{r})g(\overline{z})$, i.e. that the solution for circumferential velocity is a product of function of radius and height only, we obtain

$$\overline{V} = \frac{K\overline{r}^{\gamma-1}[\ln(1 + \overline{z}^2)]^{\gamma/2}}{(1 + \overline{r}^2)^{\gamma/2}} \tag{6}$$

$$\overline{W} = \frac{4\delta\ln(1 + \overline{z}^2)}{(1 + \overline{r}^2)^2} \tag{7}$$

Here K is a constant, and γ is an arbitrary real number. The circumferential velocity has a maximum value at

$$\overline{r}^2 = \gamma - 1 \tag{8}$$

γ is thus a parameter that can be used to generate different shapes of velocity profile. However, if we are to retain the desirable forced vortex behaviour at the tornado centre (velocity proportional to radius), and free vortex behaviour at large distances from the centre (velocity inversely proportional to radius) then we need to adopt $\gamma = 2$, which gives

$$\overline{V} = \frac{K\overline{r}[\ln(1 + \overline{z}^2)]}{(1 + \overline{r}^2)} \tag{9}$$

The peaks of both the radial and circumferential velocities are thus at a value of $\overline{r} = 1$. K is function of what we will call the swirl ratio (S) and defined here as the ratio of the maximum value of the circumferential velocity to the maximum value of the radial velocity at the reference height. (Note that this definition is similar, but not identical, to some of the definitions of swirl ratio adopted by the users of tornado vortex generators). S and K are related by

$$S = \frac{V_m}{U_m} = \left(\frac{\ln(2)}{2}\right)K = K/2.88 \tag{10}$$

and thus equation (9) becomes

$$\overline{V} = \frac{2.88S\overline{r}[\ln(1 + \overline{z}^2)]}{(1 + \overline{r}^2)} \tag{11}$$

The velocity profiles in the radial, circumferential and vertical directions are plotted in Fig. 1 below for $\bar{z} = 1$, $S = 1.0$, $\delta = 1$ and $\gamma = 2$. It can be seen that the radial and vertical velocities approach zero for large radius as is required. The circumferential profiles are compared with the earlier formulations in Fig. 2, and they can all be seen to be similar in form, although the velocities predicted by the current model lie above the other curves.

3.4. Pressure field

Normalising the radial momentum equation and ignoring the viscous terms as before we obtain

$$\bar{U}\frac{\partial \bar{U}}{\partial \bar{r}} - \frac{\bar{V}^2}{\bar{r}} + \bar{W}\frac{\partial \bar{U}}{\partial \bar{z}} = -\frac{\partial \bar{P}}{\partial \bar{r}} \tag{12}$$

where the dimensionless pressure $\bar{P}$ is given by $p/\rho u_m^2$ where p is the pressure and ρ is the density of the flow. Using equations (3), (7) and (11), the following equation for dimensionless pressure can be derived.

$$\bar{P} = -\frac{8\bar{r}^2\bar{z}}{(1+\bar{r}^2)^2(1+\bar{z}^2)^2} - \frac{4.15S^2(ln(1+\bar{z}^2))^2}{(1+\bar{r}^2)} - \frac{4ln(1+\bar{z}^2)(1-\bar{z}^2)}{(1+\bar{r}^2)^2(1+\bar{z}^2)^2} \tag{13}$$

Equation (13) is plotted in Fig. 3 for a value of $\bar{z} = 1$. It can be seen that the pressure minimum at the tornado centre is only apparent for high values of the swirl ratio S. Note also that, from equation (13), for $\bar{z} = 0$, then $\bar{P} = 0$ i.e. there is no radial pressure variation. This is clearly unrealistic and suggests that the model is not applicable in this region and some representation of the turbulent boundary layer near the ground is really required, across which the pressure will be constant in a vertical direction.

3.5. The buoyancy field

Continuing the analysis of section 3.4, we write the vertical momentum equation in dimensionless form

$$\bar{U}\frac{\partial \bar{W}}{\partial \bar{r}} + \bar{W}\frac{\partial \bar{W}}{\partial \bar{z}} = -\frac{\partial \bar{P}}{\partial \bar{z}} + \bar{F} \tag{14}$$

where $\bar{F} = Fr_m/\rho U_m^2$ and F is the buoyancy force/unit volume that actually drives the tornado. The full solution is algebraically complex, but for high values of S this has the following simple solution.

$$\bar{F} = \frac{16.6S^2 zln(1+\bar{z}^2)}{(1+\bar{r}^2)(1+\bar{z}^2)} \tag{15}$$

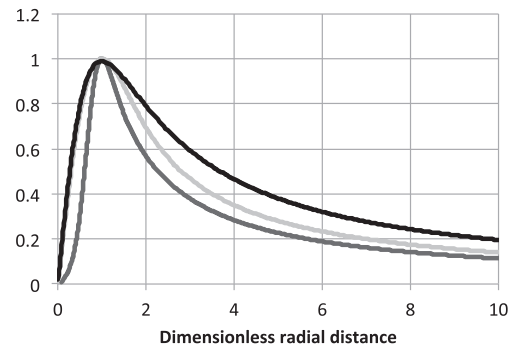This is plotted in Fig. 4 below. It can be seen that this function falls

Fig. 2. Comparison of circumferential velocity profiles (y axis is velocity divided by maximum velocity, black – new model; light grey – Burgers; dark grey – Sullivan).
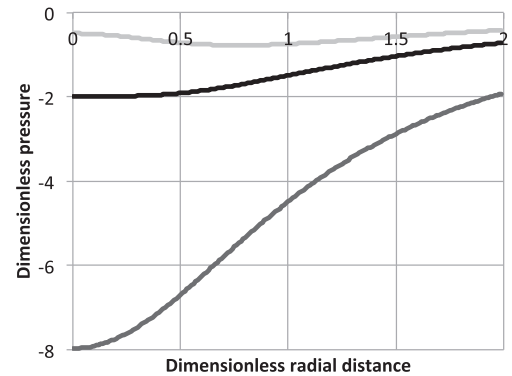
Fig. 3. Pressure distribution for different values of S ($\bar{z} = 1$; light grey $S = 0.5$, black $S = 1$, dark grey $S = 2$).

with radial and vertical distance, as seems physically reasonable.

Now it has long been recognised that the CAPE (Convection Available Potential Energy) in the atmosphere plays an important role. This is equivalent to the buoyancy force F in the present analysis. A precise equivalence is not easy to make, since CAPE is usually defined through an integration of the buoyancy between the level of free convection and the equilibrium level, neither of which are defined in the current analysis. However if we integrate the expression for buoyancy at the vortex centre, between ground level and an arbitrary height z', we can obtain an equivalent (dimensional) expression as follows for high values of S.

$$CAPE = \int_o^{z'} \frac{F(\bar{r}=0)}{\rho} = 4.2\delta S^2\left(In\left(1+\bar{z}'^2\right)\right)^2 U_m^2 \tag{16}$$

For values of $S = 1.0$, $\delta = 0.2$ (from the last section), $\bar{z}' = 5$ and

(a) Dimensionless radial velocity $\bar{U}$

(b) Dimensionless circumferential velocity $\bar{V}$

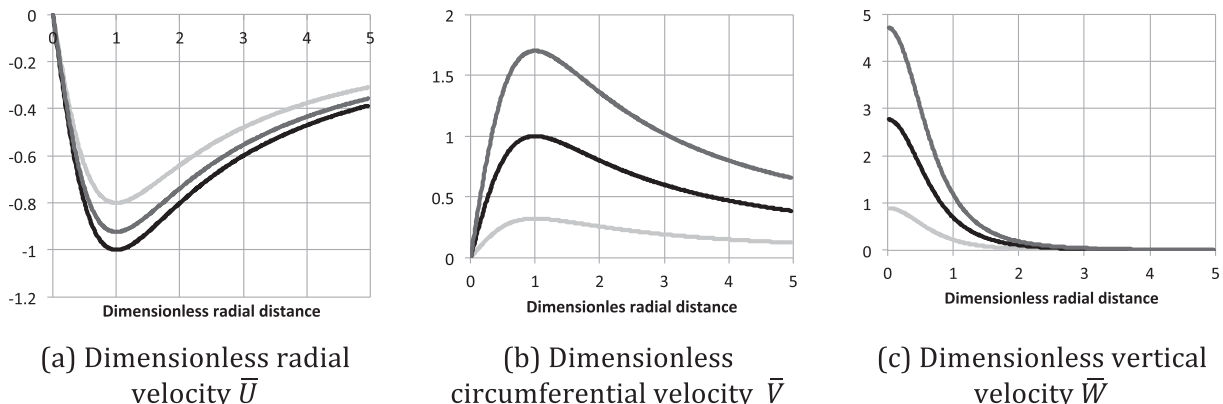(c) Dimensionless vertical velocity $\bar{W}$

Fig. 1. Velocity profiles for the new vortex model ($S = 1$, $\delta = 1$, $\gamma = 2$, light grey - $\bar{z} = 0.5$, black - $\bar{z} = 1.0$, dark grey - $\bar{z} = 1.5$.
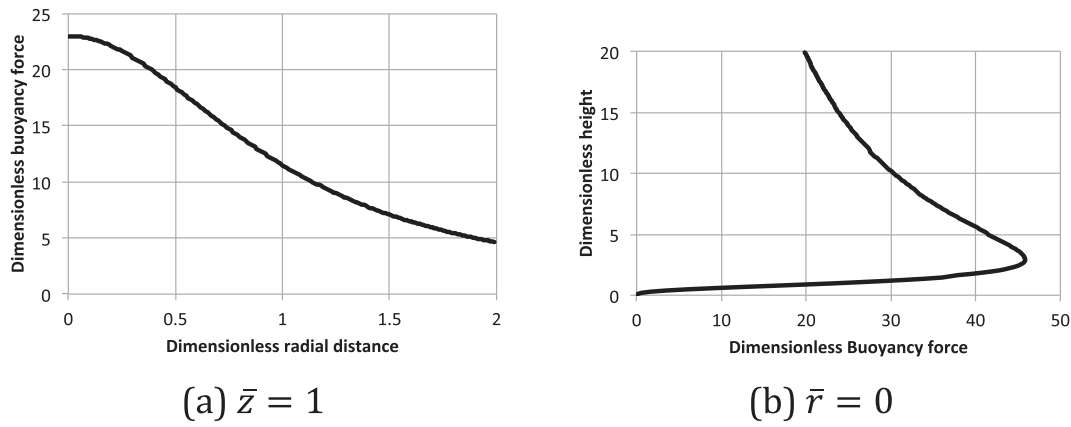
(a) $\bar{z} = 1$　　　　　　　　　　　　　(b) $\bar{r} = 0$

Fig. 4. Dimensionless Buoyancy force variation ($S = 2$).

$U_m = 20$ m/s gives a value of CAPE calculated in this way of 3.6 kJ/kg, which is consistent with the observed values for tornado formation, although the precise value is of course very dependent on the chosen parameters (Pietrycha et al., 2004).

At this point it is of interest to consider how the current modelling relates to real tornadoes. In reality tornadoes are driven by atmospheric buoyancy forces, which will control the overall magnitude of the updraft and also its geometric size. The tornado circulation is thought to be the result of a tilting of horizontal vorticity due to vertical shear. Within the tornado itself there will be a boundary layer caused by roughness near the ground. The model presented here begins with an assumption for the radial velocity, which implicitly includes a slowing down of the flow at the ground over a distance z_m, and thus allows for the boundary layer in that way (equation (3)). This assumption also defines a radial length scale r_m – the core radius. The use of the continuity equation and the circumferential momentum equation then requires the specification of the swirl ratio S, which defines the circulation, effectively as a constant of integration (equation (8) to (11)). Then through the radial and vertical momentum equations, a buoyancy force, with a radial length scale related to r_m is finally defined (Fig. 4). Thus the physical mechanisms that occur in tornadoes are present in the model, albeit not in a direct fashion. Note also that the form of the solution for the circumferential velocity in equation (6) (a product of radial and vertical functions) forces the core radius to be constant with height, which is broadly consistent with the data presented by Refan et al. (2014).

3.6. The tornado boundary layer

Clearly the issue of the thickness of the assumed tornado boundary layer needs to be addressed in some fashion, as this determines the parameter δ and thus the vertical velocity. The nature of this boundary layer will be a complex three-dimensional rotating velocity field that is not very amenable to calculation. If however one calculated the thickness of a boundary layer developing on a rough ground, using the simplified two dimensional calculation method of Gjøsund (2012), then for a (somewhat aribitrary) distance corresponding to one rotation of the tornado core, for a circumferential velocity of 50 m/s, the ratio of the boundary layer thickness to core radius (i.e. δ) is given in Table 1 for

Table 1
Approximate values of δ.

Core radius (m)	$z_0 = 0.01$ m	$z_0 = 0.1$ m	$z_0 = 1$ m
10	0.172	0.281	0.517
50	0.123	0.190	0.320
100	0.107	0.162	0.265
200	0.094	0.139	0.222

different core radii and ground roughnesses. Although very approximate, these figures suggest a value of δ of around 0.1 for smooth terrain (a 5 m boundary layer thickness for a 50 m core radius) to 0.4 for rough terrain (a 20 m boundary layer thickness for a 50 m core radius) might be appropriate. Of course the boundary layer may develop over a number of rotations of the flow, which would make these values somewhat larger. These calculations are to some degree substantiated by the model scale results of El Damatty et al. (2015) and Wang et al. (2015) which show peaks in the radial inflows at around 10–20% of the vortex core radius, but these will of course be subject to Reynolds number effects. Clearly full-scale experimental results are required to substantiate these figures and to cast some light on the nature of the tornado ground boundary layer.

3.7. Generalisation of model and two-cell formulation

As noted in section 2, full-scale tornadoes often have a two-cell structure, with a downdraft and radial outflow close to the vortex centre. In this section we develop a model for such a tornado that, whilst retaining the simplicity of the one-cell model does not however retain the full consistency with the Euler equations. We begin with a generalised form of the radial velocity assumption in equation (3) as follows.

$$\overline{U} = -\frac{(1+\alpha)(1+\beta)\bar{r}^{\alpha}\bar{z}^{\beta}}{\alpha^{\alpha/(1+\alpha)}\beta^{\beta/(1+\beta)}(1+\bar{r}^{\alpha+1})(1+\bar{z}^{\beta+1})} \tag{17}$$

The one-cell analysis took α and $\beta = 1$. As with equation (3), this equation also allows a solution of the Euler equations for the velocity and pressure. It has a maximum value of 1.0 at $\bar{r} = \alpha^{1/(1+\alpha)}$. Following the same procedure as before one obtains the following expressions for the circumferential and radial velocities.

$$\overline{V} = \frac{K\bar{r}^{\gamma-1}[\ln(1+\bar{z}^{\beta+1})]^{\gamma/(\alpha+1)}}{(1+\bar{r}^{\alpha+1})^{\gamma/(\alpha+1)}} \tag{18}$$

$$\overline{W} = \frac{\delta(1+\alpha)^2\bar{r}^{\alpha-1}\ln(1+\bar{z}^{\beta+1})}{\alpha^{\alpha/(1+\alpha)}\beta^{\beta/(1+\beta)}(1+\bar{r}^{\alpha+1})^2} \tag{19}$$

The ratio of the maximum value of circumferential velocity to the maximum value of radial velocity (the swirl ratio S) is given by

$$S = K\frac{(\gamma-1)^{(\gamma-1)/(\alpha+1)}(\ln(2))^{\gamma/(\alpha+1)}}{\gamma^{\frac{\gamma}{\alpha+1}}} \tag{20}$$

The three parameters α, β and γ allow a wide variety of consistent velocity profiles to be produced that may have some future utility when full scale measurements better define the velocity profiles. Of particular

interest are the profiles when α is large, as these give near zero values of the radial and vertical velocities close to the vortex centre, and a peak in vertical velocity away from the centre i.e. they approach a two cell solution – see Fig. 5a below.

To simulate a downdraft near the vortex core, representative of a two-cell vortex, we proceed as follows. We firstly define an additional velocity field as follows, for a downdraft with no swirl – a special case of equations (3), (7) and (11). This is again consistent with the Euler equations.

$$\overline{U} = \frac{4\tilde{r}\tilde{z}}{(1 + \tilde{r}^2)(1 + \tilde{z}^2)} \qquad (21)$$
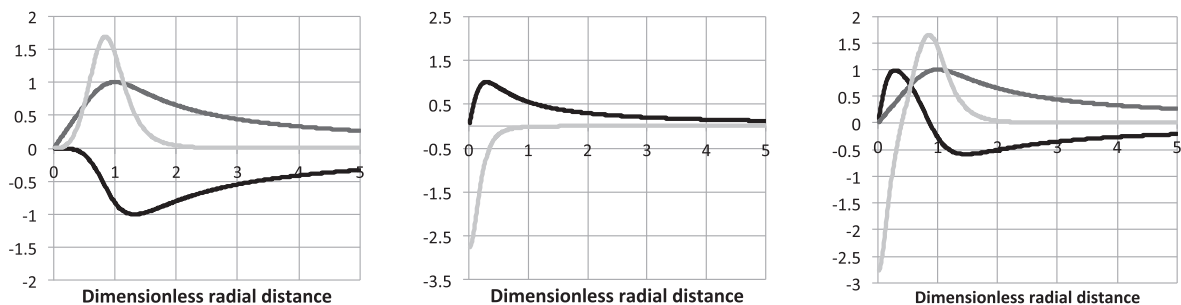
$$\overline{V} = 0 \qquad (22)$$

$$\overline{W} = -\frac{4\delta\ln(1 + \tilde{z}^2)}{(1 + \tilde{r}^2)^2} \qquad (23)$$

where $\tilde{r} = \varepsilon_r\bar{r}$ and $\tilde{z} = \varepsilon_z\bar{z}$ i.e. we introduce two new scaling factors for radial and vertical distances. This profile has a downwards velocity near the core and an outward radial velocity (see Fig. 5b). As such it may be useful for representing a downdraft such as found in thunderstorms, although it does not reproduce the transient ring vortex (see the similar work by Holmes and Oliver, 2000). Now if we add the tornado vortex profiles of equations (17)–(19) to the downdraft profiles of equations (21)–(23) we obtain the profiles shown in Fig. 5c, which give a representation of a two-cell vortex. Here we have $\varepsilon_r = 0.3$, $\varepsilon_z = 1$ i.e. the downdraft is within the core of the tornado vortex. Note that this addition violates the consistency with the Euler equations as these equations are not linear. However as a simple engineering model of a two-cell vortex with bounded velocities in the radial direction it has some merit.

3.8. Comparison with experimental results

The obvious question that arises is how well the vortex model corresponds with reality. Clearly it is only approrpiate to validate the model against full scale measurements, as CFD calculations and Tornado Vortex Generator similations are themselves models of a different form. Now, in general the available full-scale data only allows a comparison to be made with circumferential velocity data, with little consistent information available for the radial and vertical velocity components. Here we use two datasets for such a comparison.

- The velocity profiles for the Spencer tornado of 1998 given by Sarkar et al. (2005) and taken from Wurman (2002), a classic one-cell tornado near the ground, but with two cells (central downflow and outflow) at heights greater than about 80 m.

- The velocity profiles from the dataset of Refan et al. (2014) for a number of mid-strength tornadoes of varying characteristics. Here we just consider the one-cell data – the Happy 1 and Stockton 1 datasets.

The results are shown in Fig. 6. All datasets are, plotted with the velocity normalised by its maximum value, and the radius normalised by the value at which this maximum occurred. The solution of equation (12) is also shown. It can be seen that in general the model gives an upper estimate of the velocity profile, although there is much uncertainty in the measured values. Note that the existing models discussed in section 2.1 would tend to under-predict these profiles. However the nature of the comparison, with a normalisation with the maximum velocity and the radius at which this velocity occurs, means that the comparison is far from rigorous but does illustrate the potential of the model. From the data that is presented, probably the most that can be said is that the modelling presented herein is consistent with the overall form of the data. More precise verification awaits the publication of more detailed data in the future.

4. Debris flight in tornadoes

4.1. Debris flight equations

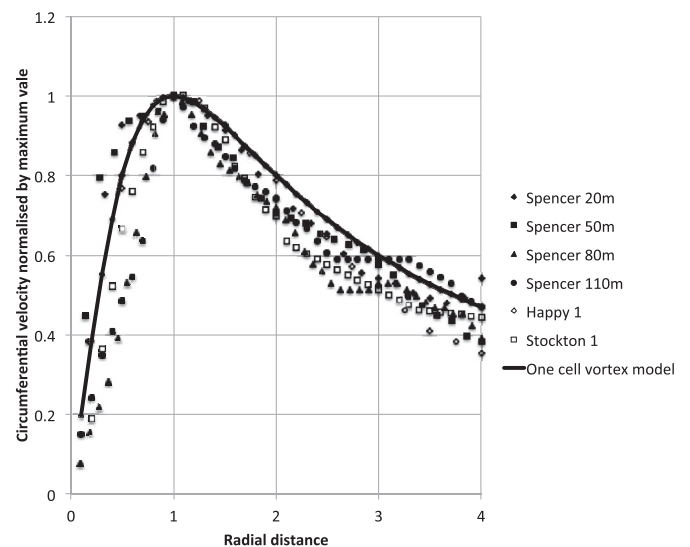Having developed a reasonably realistic model of tornado wind fields,

Fig. 6. Comparison between experimental data and equation (12) for circumferential velocity.

a) Equations 18 to 20– one-cell tornado vortex for α=4, β=1

b) Equations 21 to 23– downdraft

c) Sum of (a) and (b) – two-cell tornado vortex

Fig. 5. Approximate form for two cell tornado vortex ($\bar{z} = 1$, black – radial velocity, dark grey – circumferential velocity, light grey – vertical velocity).

we now consider the movement of debris within that wind field. It is a well known fact that wind borne debris can be of three types – compact, sheet and rod. Here we consider compact debris only, the rationale being that after a period of flight the initial perturbations tend to be damped out, and the overall forces adequately represented by a drag coefficient (C_D). This assumption is adequate for compact and sheet debris, but not for rod debris. Building on the work of Baker (2007), compact debris in a tornado wind field, the debris flight equations in the radial, circumferential and vertical wind directions are given by

$$\frac{d\bar{u}}{d\bar{t}} = \Phi \bar{R}(\bar{U} - \bar{u}) + \frac{\bar{v}^2}{\bar{r}} \tag{24}$$

$$\frac{d\bar{v}}{d\bar{t}} = \Phi \bar{R}(\bar{V} - \bar{v}) \tag{25}$$

$$\frac{d\bar{w}}{d\bar{t}} = \Phi \bar{R}(\bar{W} - \bar{w}) - \Psi \tag{26}$$

$$\bar{R} = \left((\bar{U} - \bar{u})^2 + (\bar{V} - \bar{v})^2 + (\bar{W} - \bar{w})^2 \right)^{0.5} \tag{27}$$

$$\bar{t} = \frac{t u_m}{r_m} \tag{28}$$

$$\Phi = \frac{0.5 \rho A r_m}{M} C_D \tag{29}$$

$$\Psi = \frac{g r_m}{u_m^2} \tag{30}$$

where u, v and w are the debris velocities in the radial, circumferential

and vertical directions. t is the time of flight, A is a reference area of the debris particle, M is the mass of the debris and g is the acceleration due to gravity. These are similar, although not identical to the normalised equations in Baker (2007), the differences being due to the use of tornado length and velocity scale parameters as reference lengths and velocities rather than a free stream velocity and ballast dimension as in the earlier paper. Specifically the dimensionless parameters are somewhat different and a centrifugal force term is included in equation (24).

Taken together the wind field equations (for either the one-cell or the two-cell vortex) and debris flight equations show that there are a number of parameters that control the movement of debris in tornadoes. Firstly there are those that specify the wind field – γ, δ, S and the inverse tornado Froude number Ψ. Secondly there are those that specify the initial position of the debris in the radial and vertical directions $\bar{r}_o$ and $\bar{z}_o$. Finally the buoyancy parameter Φ specifies the debris parameters. Note that this formulation does not specifically include the Tachikawa number (Holmes et al., 2006), which is often used in debris studies. This is actually the ratio Φ/Ψ, and could be included if desired. The reason for using the parameters identified here are because they are the "natural" ones to emerge form the combination of the debris flight equations and the tornado wind field. Very broadly the buoyancy parameter Φ describes the debris (small values indicating heavy debris and vice versa) and the parameter Ψ describes the strength of the tornado.

4.2. Debris trajectories for a one-cell vortex

In this section we present solutions of the above equations for two cases that represent typical debris trajectories, using the one-cell vortex velocities of equations (3), (7) and (11). In Fig. 7 we present the early stages of debris flight for the case of debris that "flies", i.e. moves
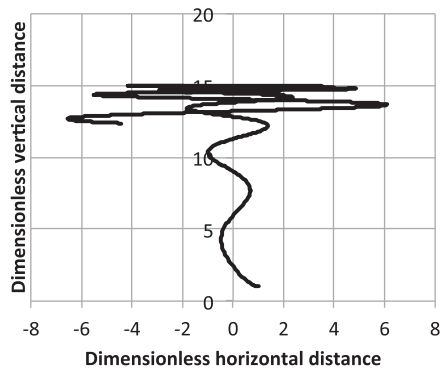
(a) Flying case ($\Phi = 50$)
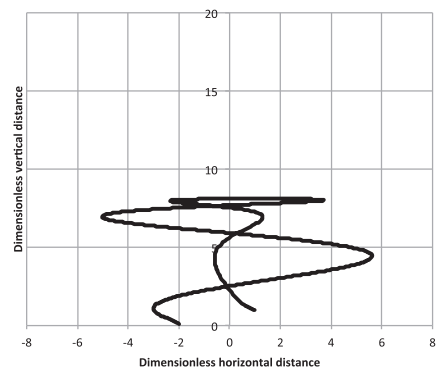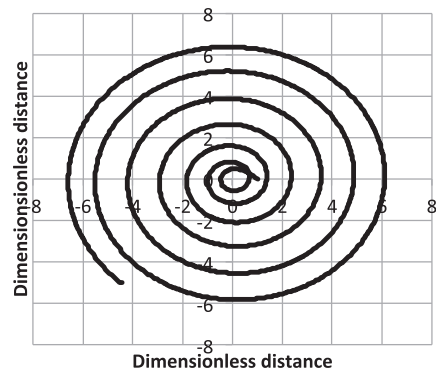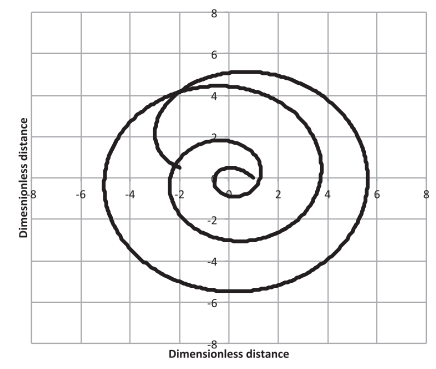

(b) Falling case ($\Phi = 10$)

Fig. 7. Early stage debris flight trajectories ($\Psi = 1$, $S = 1$, $\bar{r}_0 = 1$, $\bar{z}_0 = 1$).

vertically and stays aloft ($\Phi = 50$, $\Psi = 1$ $S = 1$, $\bar{r}_0 = 1$, $\bar{z}_0 = 1$) and for a case where debris falls to the ground ($\Phi = 10$, $\Psi = 1$ $S = 1$, $\bar{r}_0 = 1$, $\bar{z}_0 = 1$). Calculations were carried out up to a dimensionless time of 20, which corresponds to a dimensional time ranging from a few seconds to a few minutes depending on the size and strength of the tornado. The trajectories are shown in elevation and plan. For the flying case (Fig. 7a), at the start of the trajectory, the particle moves inwards and upwards, under the action of the radial and vertical velocities. As it begins to move around the tornado however, the centrifugal force grows and the particle moves outwards whilst continuing to move upwards. The particle reaches a temporary equilibrium height of $\bar{z} \approx 15$ and then begins to fall. For the falling case (Fig. 7b) the centrifugal forces dominate from the start of the trajectory, but this time the particle spirals down to ground level.

Fig. 8 shows trajectories over a much longer time scale for the flying case (up to $\bar{t} = 500$, corresponding to periods of a few minutes to an hour at full scale - the latter is of course greater than the usual tornado lifetime), plotted this time as radial and vertical positions against number of revolutions. It can be seen that the debris undergoes significant oscillations in both directions, before settling to an equilibrium position.

Fig. 9 shows the calculated boundary between the parameter range for debris flight and that for debris falling to the ground. The most significant parameters are S and Φ with the effect of variations in Ψ being less important. Again it can be seen that, as the swirl ratio increases, then only the lighter debris (higher Φ) will fly, as the centrifugal forces on the debris increase as S increases, and the debris moves outwards where the vertical velocities are lower, and is more likely to fall to the ground.

Fig. 10 shows a plot of radial against vertical debris displacement for a range of values of Φ. This is effectively a visualisation of a debris cloud that might result from a failure of a structure that releases debris of different weights and sizes, and thus different values of Φ into the tornado. It can be seen that the debris cloud has a funnel like shape and extends over considerable distances in both directions.

Fig. 11 shows how debris trajectories vary as the different dimensionless parameters vary, again plotted as radial distance against vertical distance. Firstly, it can be seen that whilst the early stage trajectories are sensitive to release position, these differences become much less marked for larger times. Secondly it seems that conversely variations in the parameter Φ are more significant in the later parts of the trajectory as the asymptotic limit is approached (see below). Finally the trajectories can be seen to be very sensitive to S with larger values of this parameter resulting in lower trajectories, due to the high centrifugal forces moving the debris rapidly to large radii and thus to regions of low vertical velocity and uplift.
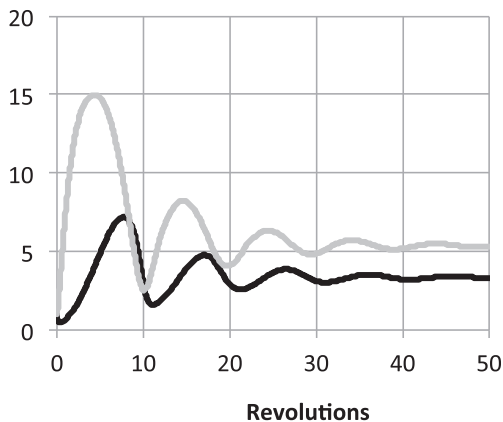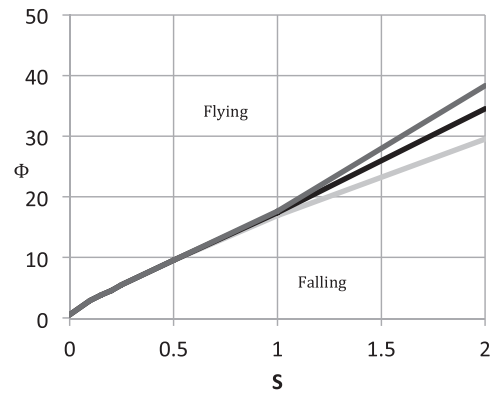

Fig. 9. Flying and falling debris parameter ranges (light grey - $\Psi = 0.5$, black - $\Psi = 1.0$, dark grey - $\Psi = 2.0$).

4.3. Asymptotic analysis for debris flight for a single cell vortex

Fig. 12 shows that the debris trajectories appear to approach an asymptotic limit for large times. It is possible to derive analytical expressions for these asymptotes as follows. For steady state solutions (no accelerations, u = U, w = W, v = V) the radial and vertical debris trajectory equations become

$$\Phi\left(\overline{U}^2 + \overline{W}^2\right)^{0.5}\overline{U} + \frac{\overline{V}^2}{\bar{r}} = 0 \tag{31}$$

$$\Phi\left(\overline{U}^2 + \overline{W}^2\right)^{0.5}\overline{W} - \Psi = 0 \tag{32}$$

since the radial and vertical debris velocities are zero, and the circumferential velocity equal to the tornado circumferential velocity. Assuming $\bar{z}^2 \gg 1.0$ and $\bar{r}^2 \gg 1.0$, then equations (3), (7) and (11) lead to

$$\overline{U} = -\frac{4}{\bar{r}\bar{z}} \quad \overline{V} = \frac{2.88Sln(\bar{z}^2)}{\bar{r}} \quad \overline{W} = \frac{4ln(\bar{z}^2)}{\bar{r}^4} \tag{33}$$

Since $\overline{W} < \overline{U}$ for the radii under consideration, the debris equations become

$$\Phi\overline{U}^2 = \frac{\overline{V}^2}{\bar{r}} \tag{34}$$

$$\Phi\overline{U}\overline{W} = \Psi \tag{35}$$

These give

Fig. 8. Long period trajectories ($\Phi = 50$, $\Psi = 1$, $S = 1$, $\bar{r}_0 = 1$, $\bar{z}_0 = 1$; black - $\bar{r}$, light grey - $\bar{z}$).
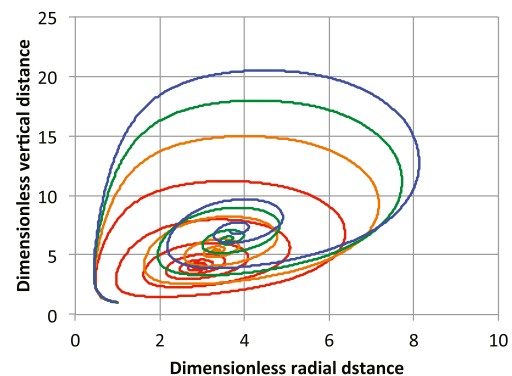

Fig. 10. Debris trajectories for a range of values of Φ ($\Psi = 1$, $S = 1$, $\bar{r}_0 = 1$, $\bar{z}_0 = 1$; red – $\Phi = 25$, brown - $\Phi = 50$, green - $\Phi = 75$, blue - $\Phi = 100$).
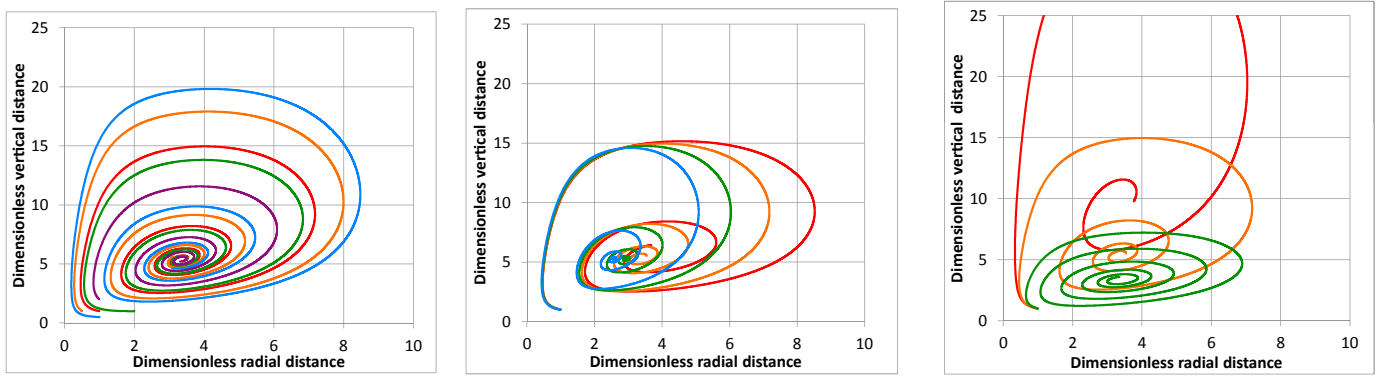
Fig. 11. Variations in debris trajectory (around $\Phi = 50$, $\Psi = 1$, $S = 1$, $\bar{r}_0 = 1$, $\bar{z}_0 = 1$).
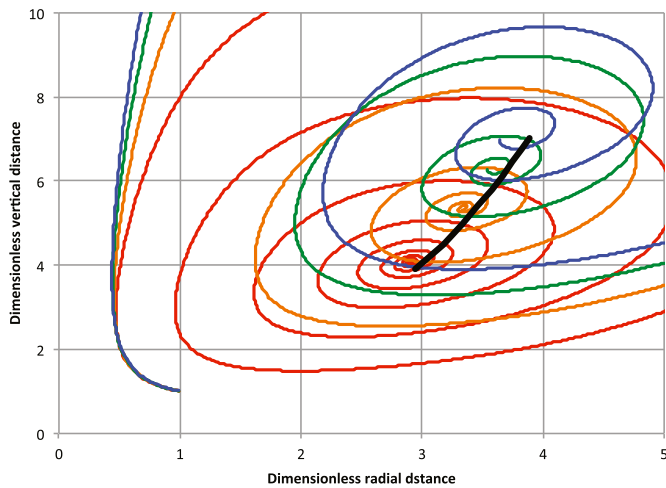

Fig. 12. Comparison of calculated debris tracks and asymptotic solution ($\Psi = 1$, $S = 1$, $\bar{r}_0 = 1$, $\bar{z}_0 = 1$; red – $\Phi = 25$, brown - $\Phi = 50$, green - $\Phi = 75$, blue - $\Phi = 100$; Asymptotic solution shown in black for Φ between 20 and 100).
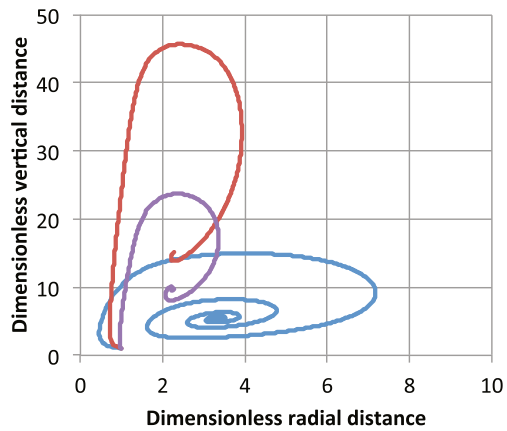

Fig. 13. Debris tracks in one and two cell vortex models ($\Psi = 1$, $S = 1$, $\bar{r}_0 = 1$, $\bar{z}_0 = 1$, $\Phi = 50$; blue – one cell vortex, $\alpha = 1$; red – one-cell vortex $\alpha = 4$; purple – two-cell vortex).

$$\bar{r} = 0.518 \left(\frac{S^2}{\Phi}\right) \bar{z}^2 \ln\left(\bar{z}^2\right)^2 \tag{36}$$

$$\bar{z}^{11/5} \ln\left(\bar{z}^2\right)^{9/5} = 3.36 \left(\frac{\Phi}{S^2}\right) \left(\frac{\Phi}{\Psi}\right)^{1/5} \tag{37}$$

For fixed values of S, Φ and Ψ, equation (36) can be solved iteratively to give $\bar{z}$ and equation (35) then solved to give a corresponding value of $\bar{r}$. Fig. 12 shows a replot of part of Fig. 9, with the asymptotic limit as calculated from the above procedure. The agreement can be seen to be good. Note that the ratio Φ/Ψ which appears in equation (36) is a form of Tachikawa number, which thus seems to be of significance in the prediction of asymptotic debris trajectories, although the exponent of 1/5 suggests that the effect of changes in this parameter will be small.

4.4. Debris tracks in two-cell vortex

The question then arises as to the nature of debris tracks in such a two-cell vortex. To investigate this, the process of section 4.2 was carried out using the model outlined in section 3.7. However, as the modelling uncertainties are significantly greater here, only a brief description of the effect on vortex tracks is presented. Fig. 13 shows plots similar to those in Fig. 9 for three cases – the standard one-cell case of Fig. 9, the one-cell case but with α changed from 1.0 to 4.0, and the full two-cell case. It can be seen there are very considerable difference in the vortex tracks, with the increase in α leading to a significantly greater equilibrium

height and smaller equilibrium radius, as the debris is caught in the updraft that is now away from the vortex centre. The full two-cell model, with the extra downdraft, lowers the equilibrium point somewhat.

5. Concluding remarks

In this paper we have, for the first time, set out simple analytical models for the velocity and pressure fields in tornado vortex and for the calculation of debris trajectories in such a vortex, and then used this model as the core component of a conceptual model for wind and debris impact loading in tornadoes. The novel developments in this modelling approach are as follows.

- A description of the velocity and pressure fields in a one-cell tornado vortex is set out, that are realistic in form, with a radial inflow and a central upflow; consistent with the Euler (high Reynolds number Navier-Stokes) equations and bounded, in that all velocity components fall to zero away from the vortex core. In these ways the model is a significant improvement over existing methods. The model is also very simple in analytical expression, and can be embedded as a component in wider models.
- A two-cell formulation is also presented, which has a rather more complex analytical expression.
- Debris trajectories within tornadoes have been modelled and the major dimensionless parameters of importance have been identified – the tornado swirl ratio, a buoyancy parameter and an inverse tornado Froude number. The parameter boundary between flying and falling debris has been identified, and the insensitivity of long period to starting conditions illustrated. The presentation of debris trajectories

in the radial/vertical plane has proved to be a powerful method of visualisation.

These very positive points being noted however, there is still work to be done before the tornado and debris can be used routinely in wind loading design, both in terms of model development and in terms of required data.

- The tornado model is weak in its treatment of the tornado boundary layer and tornado turbulence, and development is required here – although more full-scale experiments are required to inform and validate such developments.
- The debris trajectory model is at the moment only developed for compact debris. Whilst this may be a fair representation for the long-term trajectories of both compact and sheet debris, the same is probably not true for rod debris and development is needed here.

Notwithstanding these points, the analysis as presented is a potentially useful for incorporation as a component for a wider model of tornado wind loading, and a preliminary analysis of this type is set out in Baker (2016).

Funding

References

Baker, C.J., 1978. The laminar horseshoe vortex. J. Fluid Mech. 95 (2), 347–367.

Baker, C.J., 2007. The debris flight equations. J. Wind Eng. Ind. Aerod. 95, 329–353.

Baker, C.J., 2016. Tornado wind fields as experienced by a stationary observer. In: UK Wind Engineering Society Conference, Nottingham.

Brooks, H.E., Doswell, C.A., 2001. Normalized damage from major tornadoes in the United States: 1890-1999. Weather Forecast. 16 (1), 168–176.

Burgers, J.M., 1948. A mathematical model illustrating the theory of turbulence. Adv. Appl. Mech. 1, 171–199.

Bluestein, H., Lee, W.-C., Bell, M., Weiss, C., Pazmany, A., 2003. Mobile doppler radar observations of a tornado in a supercell near Bassett, Nebraska, on 5 June 1999. Part II: tornado-vortex structure. Mon. Weather Rev. 131, 2968–2984.

Case, J., Sarkar, P., Sritharan, S., 2013. Effect of low-rise building geometry on tornado-induced loads. In: 12th Americas Conference on Wind Engineering, Seattle, USA.

El Damatty, A.A., Hamada, M., Hamada, A., 2015. Simplified F2-Tornado load cases for transmission line structures. In: 14th International Conference on Wind Engineering, Porto Alegre, Brazil.

Fujita, T., 1978. Workbook of Tornadoes and High Winds for Engineering Applications. SMRP Research Paper No. 165.

Gjøsund, S.H., 2012. Simplified approximate expressions for the boundary layer flow in cylindrical sections in plankton nets and trawls. Open J. Mar. Sci. 2, 66–69.

Hangan, H., Kim, J.D., 2008. Swirl ratio effects on tornado vortices in relation to Fujita scale. Wind Struct. 11 (4), 291–302.

Haan, F.L., Sarkar, P.P., Gallus, W.A., 2008. Design, construction and performance of a large tornado simulator for wind engineering applications. Eng. Struct. 30, 1146–1159.

Hashemi-Tari, P., Gurka, R., Hangan, H., 2010. Experimental investigation of tornado-like vortex dynamics with Swirl Ratio: the mean and turbulent flow fields. J. Wind Eng. Ind. Aerod. 98, 936–944.

Holmes, J.D., Oliver, S.E., 2000. An empirical model of a downburst. Eng. Struct. 22, 1167–1172.

Holmes, J.D., Baker, C.J., Tamura, Y., 2006. Tachikawa number: a proposal. J. Wind Eng. Ind. Aerod. 94 (1), 41–47.

Ishihara, T., Oh, S., Tokuyama, Y., 2011. Numerical study on flow fields of tornado-like vortices using the LES turbulent model. J. Wind Eng. Ind. Aerod. 99, 239–248.

Jesson, M., Sterling, M., Letchford, C., Baker, C., 2015. Aerodynamic forces on the roofs of low-, mid- and high-rise buildings subject to transient winds. J. Wind Eng. Ind. Aerod. 143, 42–49.

Karstens, C.D., Samaras, T.M., Lee, B.D., Gallus, W.A., Finley, C.A., 2010. Near-ground pressure and wind measurements in tornadoes. Mon. Weather Rev. 138, 2570–2588.

Lee, A.J.H., 1974. A general study of tornado-generated missiles. Nucl. Eng. Des. 30 (3), 418–433.

Lee, J., Samaras, T., 2004. Pressure measurements at the ground in an F-4 tornado. In: 22nd Conference on Severe Local Storms. American Meteorological Society, Hyannis, Massachusetts.

Lee, W.C., Wurman, J., 2005. Diagnosed three-dimensional axisymmetric structure of the Mulhall tornado on 3 May 1999. Am. Meteorol. Soc. 62, 2373–2393.

Maruyama, T., 2011. Simulation of flying debris using a numerically generated tornado-like vortex. J. Wind Eng. Ind. Aerod. 99, 249–256.

McDonald, J.R., 1990. Impact resistance of common building materials to tornado missiles. J. Wind Eng. Ind. Aerod. 36 (2), 717–724.

Mishra, A.R., James, D.L., Letchford, C.W., 2008a. Physical simulation of a single-celled tornado-like vortex, Part A: flow field characterization. J. Wind Eng. Ind. Aerod. 96, 1258–1273.

Mishra, A.R., James, D.L., Letchford, C.W., 2008b. Physical simulation of a single-celled tornado-like vortex, Part B: wind loading on a cubical model. J. Wind Eng. Ind. Aerod. 96, 1258–1273.

Noda, M., Okamoto, R., Yamanaka, D., Hosoya, K., Nagao, F., 2015. Visualization of tornadoes based on characteristics of funnel clouds and flying debris. In: 14th International Conference on Wind Engineering, Porto Alegre, Brazil.

Pietrycha, A.E., Davies, J.M., Ratzer, M., Merzlock, P., 2004. Tornadoes in a deceptively small CAPE environment: the 4/20/04 outbreak in Illinois and Indiana. In: 22nd Conference on Severe Local Storms, Hyannis, Massachusetts: American Meteorological Society.

Redmann, G.H., Radbill, J.R., Marte, J.E., Degarabedian, P., Fendell, F.E., 1976. Wind Field and Trajectory Models for Tornado-propelled Objects. Technical Report 1. Electrical Power Research Institute, Palo Alto, CA.

Refan, M., Hangan, H., Wurman, J., 2014. Reproducing tornadoes in laboratory using proper scaling. J. Wind Eng. Ind. Aerod. 135, 136–148.

Refan, M., Hangan, H., 2016. Characterization of tornado-like flow fields in a new model scale wind testing chamber. J. Wind Eng. Ind. Aerod. 151, 107–121.

Rott, N., 1958. On the viscous core of a line vortex. Z. Angew. Math. Phys. 9, 543–553.

Sarkar, P., Haan, F., Gallus, W., Le, K., Wurman, J., 2005. Velocity measurements in laboratory tornado simulator and their comparison with numerical and full scale data. In: 37th Joint Meeting Panel on Wind and Seismic Effects, Tsubuka, Japan.

Sullivan, R.D., 1959. A two-cell vortex solution of the Navier–Stokes equations. J. Aerosp. Sci. 46, 767–768.

Tachikawa, M., 1988. A method for estimating the distribution range of trajectories of wind-borne missiles. J. Wind Eng. Ind. Aerod. 29, 175–184.

Tamura, Y., Matsui, M., Kawana, S., Kobayashi, F., 2015. Statistical properties of tornadoes in Japan and tornado risk model for nuclear power plants. In: 14th International Conference on Wind Engineering, Porto Alegre, Brazil.

Twisdale, L.A., Dunn, W.L., Davis, T.L., 1979. Tornado missile transport analysis. Nucl. Eng. Des. 51 (2), 295–308.

USNRC, 2007. Design Basis Tornados and Tornado Missiles for Nuclear Power Plants. US Nuclear Regulatory Commission.

Wang, J., Cao, S., Pang, W., Cao, J., Zhao, L., 2015. The effects of ground roughness on the characteristics of tornado-like vortices. In: 14th International Conference on Wind Engineering, Porto Alegre, Brazil.

Wood, V.T., Brown, R.A., 2011. Simulated tornadic vortex signatures of tornado-like vortices having one- and two-celled structures. J. Appl. Meteorol. Climatol. 50, 2338–2342.

Wurman, J., Gill, S., 2000. Finescale radar observations of the dimmitt, Texas (2 June 1995) tornado. Mon. Weather Rev. 128, 2135–2164.

Wurman, J., Straka, J.M., Rasmussen, E.N., 1996. Fine-scale doppler radar observations of tornadoes. Science 272, 1774–1777.

Wurman, J., 2002. The multiple vortex structure of a tornado. Weather Forecast. 17, 473–505.

Xu, Z., Hangan, H., 2009. An inviscid solution for modeling of tornado-like vortices. ASME J. Mech. 76, 031011.